

# Dynamical windows for real-time evolution with matrix product states

Ho N. Phien,<sup>1</sup> Guifré Vidal,<sup>2</sup> and Ian P. McCulloch<sup>1</sup>

<sup>1</sup>*Centre for Engineered Quantum Systems, School of Mathematics and Physics,  
University of Queensland, Brisbane 4072, Australia*

<sup>2</sup>*Perimeter Institute for Theoretical Physics, Waterloo, Ontario, N2L 2Y5, Canada*

(Dated: August 22, 2021)

We propose the use of a dynamical window to investigate the real-time evolution of quantum many-body systems in a one-dimensional lattice. In a recent paper [H. Phien et al, arxiv:????????], we introduced infinite boundary conditions (IBC) in order to investigate real-time evolution of an infinite system under a local perturbation. This was accomplished by restricting the update of the tensors in the matrix product state to a finite window, with left and right boundaries held at fixed positions. Here we consider instead the use of a dynamical window, namely a window where the positions of left and right boundaries are allowed to change in time. In this way, all simulation efforts can be devoted to the space-time region of interest, which leads to a remarkable reduction in computational costs. For illustrative purposes, we consider two applications in the context of the spin-1 antiferromagnetic Heisenberg model in an infinite spin chain: one is an expanding window, with boundaries that are adjusted to capture the expansion in time of a local perturbation of the system; the other is a moving window of fixed size, where the position of the window follows the front of a propagating wave.

PACS numbers: 03.67.-a, 03.65.Ud, 02.70.-c, 05.30.Fk

## CONTENTS

I. Introduction	1
II. Dynamical window techniques	2
A. Window Expansion	2
B. Window Contraction	3
C. Moving window criteria	3
III. Numerical Calculations	4
A. Expanding window	4
B. Moving window	5
IV. Conclusion	6
Acknowledgments	7
References	7

## I. INTRODUCTION

Ever since the density-matrix renormalization group method (DMRG)<sup>1,2</sup> was invented in 1992 by Steven R. White, it has opened new trends for studying numerically strongly correlation effects of quantum systems in one dimension. By now, it is well established as a powerful method in producing numerically exact results for ground state wavefunctions and expectation values of one-dimensional quantum systems. In addition, the DMRG is not constrained itself within a small regime for investigating static properties but it has been extended to study dynamical properties<sup>3-6</sup> as well as quantum systems at finite temperature<sup>7,8</sup>.

The connection was not immediately made that the wavefunction produced by DMRG can be realized as

a variational calculation in the space of matrix product states (MPS)<sup>9-11</sup>. As it is much simpler and easier, generally people prefer to implement the DMRG in terms of MPS. Furthermore, together with MPS the tensor network (TN) ansatz have been attracting much interest from computational physicists. Algorithms have developed based on MPS to simulate both static and dynamical properties of 1D quantum systems. One of the most successful algorithms in MPS formalism is the time-evolving block decimation (TEBD) algorithm<sup>12,13</sup>, which has an equivalent DMRG formulation<sup>14,15</sup>. This algorithm can be used for ground state calculations, although it is not as efficient as variational minimization algorithms such as DMRG. However TEBD comes into its own for real-time evolution. More recently, a new algorithm called the time-dependent variational principle (TDVP)<sup>16</sup> has also been introduced.

There are many interesting problems that involve dynamics of a small section embedded in an infinite lattice. For example, consider the real-time evolution of an infinite quantum spin chain after one site in the middle of the chain has been locally perturbed by some spin excitation, e.g. a local  $S^+$  operator. The ground state is now modified and become a superposition of excited states. Therefore the infinite MPS (iMPS) cannot be represented in a translationally invariant form anymore. This is a huge hurdle to investigate real-time evolution of the system in thermodynamic limit, as in principle one must use an infinite set of different tensors in the iMPS to describe the wave function of the state. This makes the simulation an impossible task. However, because the perturbation is local, one can avoid this difficulty and can still understand the dynamical properties of a system in thermodynamic limit, as long as the range of effect is finite (or approximately so). The conventional way to solve this problem

is to use a large, but finite lattice chosen to be large enough that the boundaries are far enough away to not cause problems for the calculation. As the wavefunction evolves in time, this local perturbation represented by a wave-packet will spread throughout the system at the group velocity (for ballistic transport) or slowly spread out through the system (in the diffusive case). Thus, to obtain the long-time evolution of a system in this way the lattice size must be fairly large, firstly to avoid Friedel oscillations from the boundaries affecting the ground state, and also for the time evolution the simulation typically needs to stop once the wave front approaches the boundary. In a previous paper<sup>18</sup> we have shown how the computational cost can be substantially improved by using a much smaller finite system with infinite boundary conditions (IBC). This has two advantages, firstly there is no hard boundary in the system, so no Friedel oscillations, and away from the perturbation the system is asymptotically translationally invariant; and secondly, since the ‘boundaries’ of the finite system represent an effective semi-infinite chain rather than a hard wall, there is no problem to allow the perturbation to propagate beyond the finite region as long as the wavefunction doesn’t move too far outside the effective Hilbert space of the semi-infinite chain. This is a big advantage over traditional finite-size calculations. To achieve this, we divide the whole spin chain into three parts where the middle part contains the perturbation, called the *window*, and other two parts on the left and right of its which are not affected by the perturbation. The boundaries of the window are represented by an effective Hilbert space for the wave function on a semi-infinite strip.

In this paper, we further improve the computational efficiency of the IBC technique by focusing on how the wavefront propagates in time. Efficiencies can be obtained by introducing dynamical window techniques, namely expanding and moving the window throughout the calculation. Specifically, we will keep track of the wavefront and decide to expand or move the window such that the physically relevant section of the system is well represented. An important point is that in our scheme the section of the system outside of the window, represented by an effective Hilbert space, can evolve as well so that the window size can be quite small, containing only on the region of interest, without affecting the accuracy too much. An Results are presented for a the evolution of a local perturbation in the spin-1 antiferromagnetic (AFM) Heisenberg model.

## II. DYNAMICAL WINDOW TECHNIQUES

Let us consider an infinite spin chain where the ground state is represented by a translationally invariant infinite matrix product state (iMPS) with a one-site unit cell,

$$|\Psi\rangle = \sum_{s_i} \dots \lambda \Gamma^{s_i} \lambda \Gamma^{s_{i+1}} \dots |s\rangle, \quad (1)$$

where  $|s\rangle = |\dots s_i, s_{i+1} \dots\rangle$  is the basis in Hilbert space  $\mathcal{H} \in \mathbb{C}^{\otimes d}$  of the system ( $d$  is the dimension of local Hilbert space at each lattice site). This iMPS can be always written in the mixed canonical form as following

$$|\Psi\rangle = \sum_s \dots A^{s_{i-1}} A^{s_i} \lambda B^{s_{i+1}} B^{s_{i+2}} \dots |s\rangle, \quad (2)$$

where tensors  $A$  and  $B$  satisfy the canonical form constraints

$$\sum_{s_i} A^{s_i \dagger} A^{s_i} = \sum_{s_i} \Gamma^{s_i \dagger} \rho^R \Gamma^{s_i} = \mathbb{I}, \quad (3)$$

$$\sum_{s_i} B^{s_i} B^{s_i \dagger} = \sum_{s_i} \Gamma^{s_i} \rho^L \Gamma^{s_i \dagger} = \mathbb{I}, \quad (4)$$

where  $\mathbb{I}$  is identity matrix,  $\rho^L$  and  $\rho^R$  are the left and right reduced density matrices, respectively.

After perturbing the ground state, the infinite spin chain can be described effectively by the finite MPS as,

$$|\tilde{\Psi}\rangle = \sum_{\{s_i\}} L^\alpha A_1^{s_1} \lambda A_2^{s_2} \dots A_N^{s_N} R^\beta |\alpha, \tilde{s}, \beta\rangle, \quad (5)$$

where  $|\tilde{s}\rangle = |s_1, s_2, \dots s_N\rangle$ ,  $A_1^{s_1}$  fulfills the condition in Eq. 3 and all the other tensors on the right of  $\lambda$  matrix satisfy the right canonical constraint in Eq. 4. Calculation for corresponding effective Hamiltonian of this system was described in Ref. 18 as was the scheme for evolving the system in time using TEBD algorithm. Here, we reuse these techniques combining with the dynamical window technique to investigate the dynamical properties of the system. Dynamically changing the window size involves two basic steps, contraction of the window and expansion of the window. We now describe the technical steps involved in each case.

### A. Window Expansion

Expanding the window incorporates more degrees of freedom into the variational wavefunction, and this is an operation that one will typically want to do in order to follow the propagation of a perturbation as it travels through the lattice. This is achieved by incorporating some sites from the translationally-invariant semi-infinite chain into the finite-size window. The window can be expanded on the left and the right hand side separately, for example to follow the wavefront of a symmetrically-expanding local perturbation we use the scheme in Fig. 1. The basic operation on the the MPS, from Eq. 5 becomes, in the case of a two-site unit cell expanding on the left-hand side,

$$|\tilde{\Psi}\rangle = \sum_{s_i} L^\alpha A_{-1}^{s_{-1}} A_0^{s_0} A_1^{s_1} \lambda A_2^{s_2} \dots A_N^{s_N} |\alpha \tilde{s}' \beta\rangle, \quad (6)$$

$$(7)$$

where the initial values of the tensors  $A_{-1}$  and  $A_0$  are simply given by the translationally-invariant matrices  $A$

of the ground state Eq. 2. Note that the Hilbert space  $|\alpha\rangle$  at the left edge of the window is unchanged. Therefore the block operators acting on this space are also unchanged, although care needs to be taken that the energy of the system is correctly taken into account. In calculating the effective Hamiltonian<sup>18</sup>, the energy per site of the infinite system appears as a separate term which is easily removed. Thus, in order for the total energy of the system to remain constant as the window is expanded, it is convenient to subtract this energy off the Hamiltonian for the finite window as well. This amounts to subtracting the ground state energy per site off the window Hamiltonian for each site added to the window.

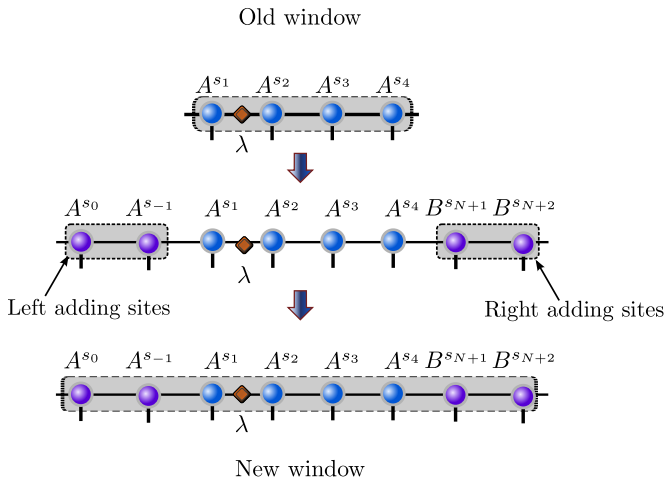


FIG. 1. (Color online): Diagrammatic representation of adding the sites into both sides of the window for the window expansion step.

### B. Window Contraction

The second operation that we can perform on the window is to contract the size of it, by absorbing some sites of the window into the boundary tensor. To achieve this, we contract over those sites to obtain a new set of block operators and effective Hamiltonian that will now describe a semi-infinite chain plus some number of additional (not translationally invariant) sites. This procedure is implemented as shown in Fig. 2. The components of the block operators become, for example on the right-hand side,

$$E'_R = \sum_{s_N} \sum_{s_{N-1}} A^{s_{N-1}\dagger} A^{s_N\dagger} E_R A^{s_N} A^{s_{N-1}} \langle s_N | W | s_N \rangle \langle s_{N-1} | W | s_{N-1} \rangle, \quad (8)$$

where  $W$  is the matrix product operator (MPO) of the Hamiltonian of the system. The tensors  $A^{s_N}$  and  $A^{s_{N-1}}$  satisfy the right canonical form constraint in Eq. 4 and in the Fig.8, they are  $A^{s_4}$  and  $A^{s_3}$ , respectively.

Again, one needs to take care that the total energy of the system is unchanged in this procedure, which is easily

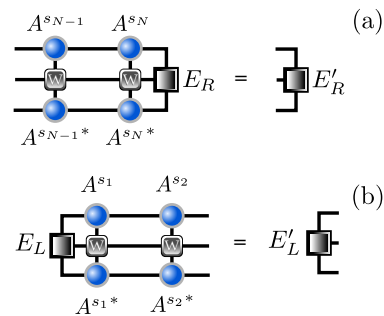


FIG. 2. (Color online): Updating the effective Hamiltonian for contracting the window size. (a). Right update is performed when incorporating sites from the right-hand edge of the window into the right boundary. (b). Left update for incorporating sites from the left-hand edge of the window into the left boundary.

effected by adding a constant equal to the ground state energy per site to the Hamiltonian of the window.

### C. Moving window criteria

Now we will explain the criteria when to expand or move the window. There are many ways to do this, for example, from the result of fixed window, we can look at how the wavefront propagates in time and determine the maximum velocity of excitations. However, it is much more convenient to use another criteria that relies on the fidelity of the tensors which include  $A^{s_1}$  and  $\lambda$  matrices between two successive time steps at the edge of the window. We do this by measuring how much the reduced density matrix changes from one time-step to the next. Assume that at time  $t$  the MPS is described by Eq. 5 with the reduced density matrix  $\rho^R = \lambda^2$  and later time  $t + \delta t$  is represented by

$$|\tilde{\Psi}'\rangle = \sum_{s_i} B^{s_1} \lambda' B^{s_2} B^{s_3} \dots B^{s_N} |\tilde{s}\rangle, \quad (9)$$

where the new reduced density matrix  $\rho^{R'} = \lambda'^2$ . If two tensors  $A^{s_1} \lambda$  and  $B^{s_1} \lambda'$  are the same then  $\rho^{R'} = \rho^R$ . What we want to check is the fidelity of these two density matrices,

$$\sqrt{F}(\rho^{R'}, \rho^R) = \text{tr} \sqrt{\sqrt{\rho^R} \rho^{R'} \sqrt{\rho^R}} \quad (10)$$

This fidelity is obtained as the sum of the singular values of

$$\sum_{s_1} (B^{s_1} \lambda')^\dagger A^{s_1} \lambda = U S V^\dagger. \quad (11)$$

If this fidelity is close to 1 then we can conclude that these tensors are the same and we do not need to move the window. Typically, we use a threshold of  $1 - 10^{-4}$  in our numerical calculations.

### III. NUMERICAL CALCULATIONS

Now we explain in detail how to calculate the observables of the system during the time evolution of the system with increasing window size. The two observables that we are interested in are: local magnetization  $\langle S^z(x, t) \rangle$  ( $x$  is the position of the lattice site) in which we can see how the wave packet propagates in time and un-equal time two-point correlator  $\langle A(x, t) \rangle$  from which one can extract the spectral function. We calculate these observables for two different dynamical window schemes; an expanding window, where we increase the size of the window symmetrically to encompass the symmetrically expanding wavefronts, and a moving window where we take the window to be much smaller, to test the case where one is interested mainly in the dynamics of a small section of a larger system. In the latter case, a significant amount of the dynamics will occur outside of the window, so an important test of the method is to check that the dynamics within the window remains accurately described. In this section, we present results for the spin-1 AFM Heisenberg model. Simulation has been implemented with  $\chi = 200$  where  $\chi$  is number of states kept in TEBD. The time step is  $\delta t = 0.05$  and we have used fourth order Suzuki-Trotter expansion<sup>17</sup>.

#### A. Expanding window

We start the time evolution of the system with a small window size  $N_e$  in which the perturbation appears in the middle at position  $N_e/2$  from the left. Outside the window, the MPS tensors are position-independent. The expanding window scheme is illustrated in Fig. 3. The starting window contains  $N_e = 4$  lattice sites and then increases with time. We can see that when the wavefront hits boundaries, the window moving criteria is met so we need extend the window by adding some number of unit cells to both sides of the window. Here we add one two-site unit cell at a time, however in principle, we can add as many unit cells as we want. After adding the sites, we evolve the system for some more time before the next expanding procedure.

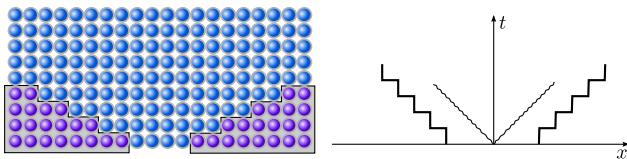


FIG. 3. (Color online): Illustration of how the window is expanded in time and space. The balls are represented for the lattice sites on the left figure. Blue balls are inside the windows and outside the window, translationally invariant purple balls are used. On the right figure, the wavefront is moving in time while the window is expanded along the spin chain axis.

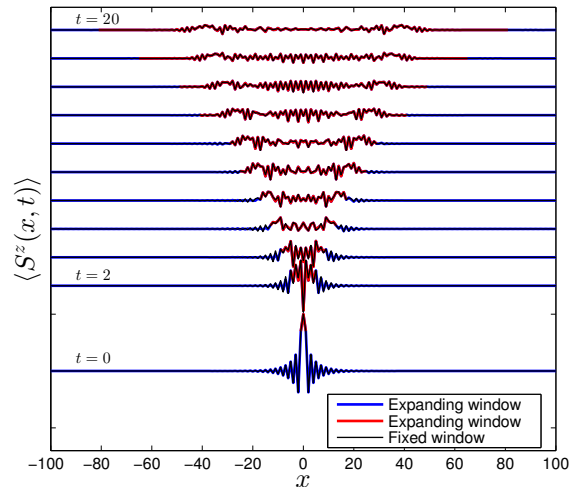


FIG. 4. (Color online): Comparison of wave-packet propagating in time between different schemes: fixed and expanding window.

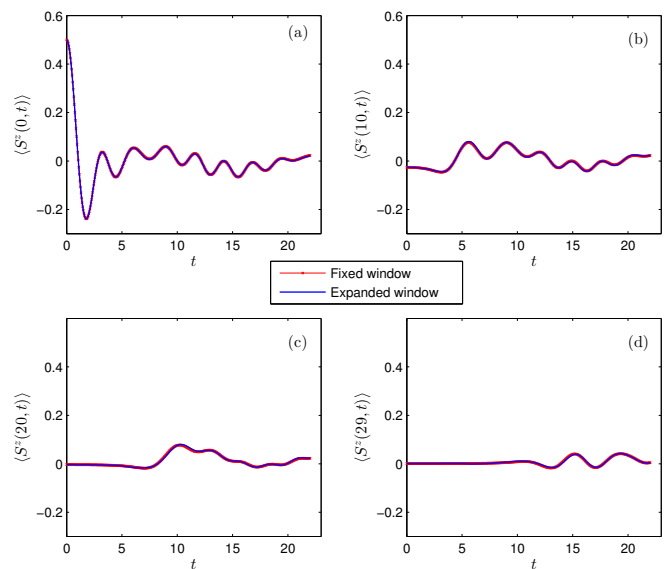


FIG. 5. (Color online): Comparison of local magnetization evolving in time at specific positions  $x_j$  between different schemes: fixed and expanded window. (a).  $x_j = 0$ ; (b).  $x_j = 10$ ; (c).  $x_j = 20$ ; (d).  $x_j = 29$ .

Fig. 4 shows our numerical calculation of  $\langle S^z(x, t) \rangle$ . It also shows the result calculated for the case of time-evolving fixed window of size  $N_f = 240$  for comparison (this is numerically exact for these purposes). It can be seen that the results obtained from the different methods are almost the same although the size of starting window is small and increasing slowly in time. Of course, the expanding window calculation is much faster because the computation time is essentially linear in the size of the finite window.

In order to see how different the wave packets between expanded and fixed window methods are, we plot the

local magnetization  $\langle S^z(x_j, t) \rangle$  at different positions  $x_j$  corresponding to the initial local perturbation position of equivalent lattice sites. The results are shown in Fig. 5,  $x_j = \{0, 10, 20, 29\}$ . We can see that they match very well. For a better understanding, we plot of absolute difference between two methods in Fig. 6. By now it can be seen that these differences increases with time. However, they all oscillate around an acceptably small value  $\sim 10^{-4}$ .

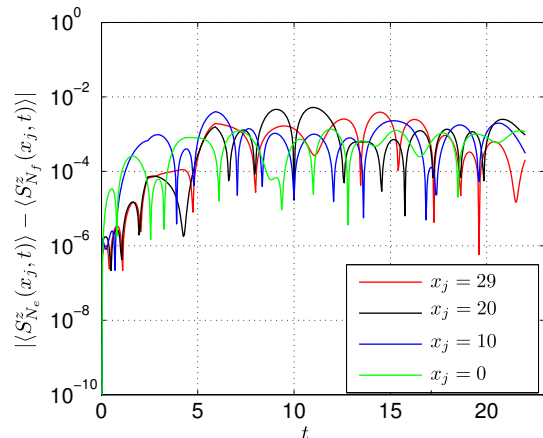


FIG. 6. (Color online): Difference in local magnetizations evolving in time at specific positions  $x_j$  between different schemes: fixed and expanding window.

## B. Moving window

We now discuss another scheme of dynamical window technique, which combines the expansion and contraction steps to obtain a fixed-size but moving window. The window is now fixed in size and is shifted along the chain as soon as the wavefront hits boundary. In principle, we can move this window to either sides of chain. In Fig. 7, the initial small-size window which contains  $N = 4$  sites and is located on the left most side of the finite chain. As the wavefront propagates in time, this window will move to the left of the spin chain. As a consequence of this, on the right side of the window, the wavefront will hit boundary after some time but on the left side the wavefront doesn't hit the boundary. Therefore, all the information of dynamical properties measured in the area containing blue and purple balls should be reliable, but the wavefunction in the black region will be obtained only in a small effective Hilbert space.

The advantage of this scheme is that it is very cheap in computational cost as we just need to modify and update the sites inside the window. To understand how it is implemented in terms of tensor network, we introduce the update scheme for MPS and effective Hamiltonian before the window is shifted to a new position. There are two most important components in the update scheme of the real-time evolution algorithm of the MPS with infinite

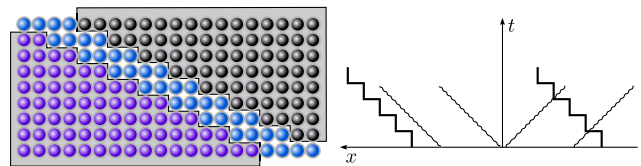


FIG. 7. (Color online): Illustration of how the window is shifted in time and space. The balls are represented for the lattice sites of the left figure. Inside the windows blue balls are used. On the left side the window, translationally invariant purple balls are used. The black balls corresponds to the blue balls at the same positions of the chain before moving the window. Figure on the right shows the wavefront moving in time along the space while the window is shifted.

boundary conditions.

The procedure for updating the new window contained in the MPS is described in Fig. 8. When the moving window criteria is met, we need to shift the window to the left by one two-site unit cell. Note that the number of sites in the old window that are absorbed into the right boundary is equal to the number of added sites to make sure that the size of the new window is as same as the old one.

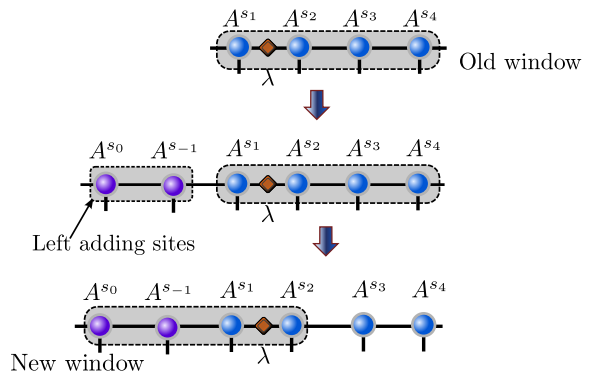


FIG. 8. (Color online): Illustration of how to update the MPS when moving the window to the left of the spin chain.

Again, we investigate the local magnetization  $\langle S^z(x, t) \rangle$  and compare with the result obtained for the fixed window case. The comparison is plotted in Fig. 9. In our numerical calculation the window size of moving window scheme is chosen to be  $N_m = 8$  compare to the size of fixed window  $N_f = 240$ . We can see that the moved window captures well the wavefront propagating to the left of the chain and fit nicely with the case of fixed window. Therefore, we have obtained most of the dynamical information of interest, with a calculation that is an order of magnitude more efficient than choosing a large fixed window, and therefore *much* more efficient than the traditional method for performing this calculation, namely a large finite system with open open boundary conditions.

We now examine the local magnetizations at some specific positions of the spin chain. In Fig. 10, we plot

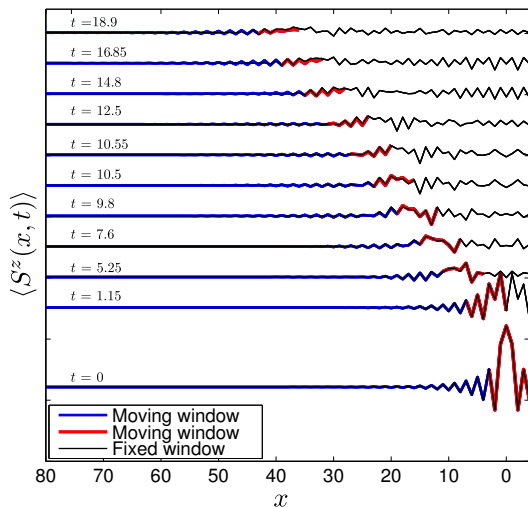


FIG. 9. (Color online): Comparison of wave-packet propagating in time between different schemes: fixed and moved window. The black lines corresponds to the fixed window with size  $N_f = 240$ . The red and blue lines correspond to the cases of inside and outside of the moved window size  $N_m = 8$ , respectively.

$\langle S^z(x_j, t) \rangle$  at  $x_j = \{0, 10, 20, 29\}$ . We can see that in all of four sub-plots  $\langle S^z(x_j, t) \rangle$  of moved window fit quite well with the data from the case of fixed window. Especially, the further away from the initial perturbation point, the longer the time scale for which we can obtain accurate results. This is easy to understand as it takes longer time for the window to move to the further sites of the chain, and the region to the left of the chain is well-described by the Hilbert space of the semi-infinite chain. When the window passes through a region of the lattice, these sites will eventually be absorbed into the right boundary, so this causes the results measured after that time to be less accurate. That is the reason why we see a big deviation of the results after some time.

For a clearer comparison of  $\langle S^z(x_j, t) \rangle$ , we also plot the difference between two schemes in Fig. 11. We can see that at the early time the differences seem to be small and then increase in time. These errors can be well-controlled by manipulating the size of the window and the criteria for moving the window.

#### IV. CONCLUSION

We have introduced two dynamical window techniques for studying the real-time evolution of a locally perturbed infinite spin chain, the expanding window and the moving window. Taking advantage of infinite boundary conditions which has been introduced to replace an infinite MPS by a finite MPS, we have proved that these two techniques are viable and are a more efficient replacement for the fixed window technique.

One of the great advantages of these techniques a large

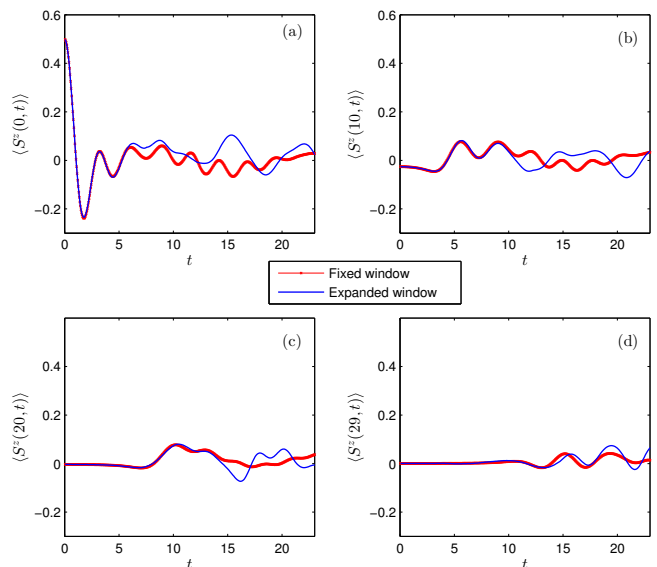


FIG. 10. (Color online): Comparison of local magnetization evolving in time at specific positions  $x_j$  on the left side of perturbation point between different schemes: fixed and moving window. The size of fixed window is  $N_f = 240$  and  $N_m = 8$  for the moving window. (a).  $x_j = 0$ ; (b).  $x_j = 10$ ; (c).  $x_j = 20$ ; (d).  $x_j = 29$ .

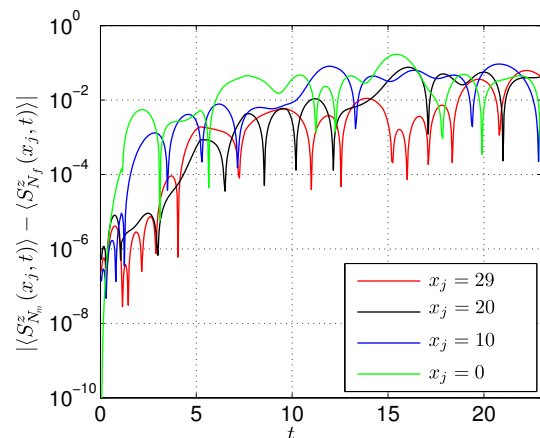


FIG. 11. (Color online): Difference in local magnetizations evolving in time at specific positions  $x_j$  on the left side of perturbation point between different schemes: fixed and moved window.

saving in computational resource as we only need to compute the evolution of a small window of the system. This is most significant for the moving window technique, where the computational cost per time-step doesn't increase as the perturbation propagates through the system. This is particularly relevant for cases where the physically relevant dynamics of the system is a small region, for example in the vicinity of the wave-front. For calculating quantities such as the spectral function, we are interested in regions only where the correlation function differs significantly from zero, so this approach,

where the dynamics are obtained accurately in a small region and approximated elsewhere, is a significant improvement.

the Australian Research Council Centre of Excellence for Engineered Quantum Systems and the Discovery Projects funding scheme (project number DP1092513).

### ACKNOWLEDGMENTS

During preparation of this manuscript we learned of some related works<sup>19,20</sup>. We acknowledge support from

- 
- <sup>1</sup> S. R. White, Phys. Rev. Lett. **69**, 2863 (1992)  
<sup>2</sup> S.R. White, Phys.Rev. B **48**, 10345 (1993)  
<sup>3</sup> K. Hallberg, Phys. Rev. B **52**, R9827 (1995)  
<sup>4</sup> T.D. Kühner and S.R. White, Phys. Rev. B **60**, 335 (1999)  
<sup>5</sup> E. Jeckelmann, Phys. Rev. B **66**, 45114 (2002)  
<sup>6</sup> M. A. Cazalilla and J. B. Marston, Phys. Rev. Lett. **88**, 256403 (2002)  
<sup>7</sup> X. Wang und T. Xiang, Phys. Rev. B **56**, 5061 (1997)  
<sup>8</sup> J. Sirker, Phys. Rev. B **71**, (2005)  
<sup>9</sup> S. Ostlund and S. Rommer, Phys. Rev. Lett. **75**, 3537 (1995)  
<sup>10</sup> M. Fannes, B. Nachtergaele and R. Werner, Commun. Math. Phys. **144**, 443 (1992)  
<sup>11</sup> D. Perez-Garcia, F. Verstraete, M.M.Wolf and J.I.Cirac, Quantum Inf. Comput. **7**, 401 (2007)  
<sup>12</sup> G. Vidal, Phys. Rev. Lett. **91**, 147902 (2003)  
<sup>13</sup> G. Vidal, Phys. Rev. Lett. **93**, 040502 (2004)  
<sup>14</sup> S. R. White, A. E. Feiguin, Phys. Rev. Lett. **93**, 076401 (2004)  
<sup>15</sup> A. J. Daley, C. Kollath, U. Schollwoeck and G. Vidal, J. Stat. Mech.: Theor. Exp. (2004) P04005.  
<sup>16</sup> J. Haegeman, B. Pirvu, D. J. Weir, J. I. Cirac, T. J. Osborne, H. Verschelde, F. Verstraete, Phys. Rev. B **85**, 100408(R) (2012)  
<sup>17</sup> N. Hatano and M. Suzuki, arXiv:math-ph/0506007v1  
<sup>18</sup> H. N. Phien, Ian P. McCulloch and G. Vidal, arXiv:????????  
<sup>19</sup> V. Zauner, M. Ganahl, H. G. Everts and T. Nishino, arXiv:????.????  
<sup>20</sup> A. Milsted and T. J. Osborne, arXiv:????????